
Watch Your Step: Information Injection in Diffusion Models via Shadow Timestep Embedding

An Huang¹ Junggab Son¹ Zuobin Xiong¹

Abstract

Diffusion models have become the foundation of modern generative systems, with most research focusing primarily on improving generation efficiency and output quality. The timestep embedding component is a crucial part of the diffusion pipeline, which provides a temporal conditioning signal to the denoising network, enabling it to adapt its predictions across different noise levels throughout the process. Despite their potential to contain substantial information, timestep embeddings remain underexplored in current research, especially for security risks and reliable provenance. To fill this gap, we introduce **Shadow Timestep Embedding (STE)**, a novel mechanism that investigates the underutilized temporal space for malicious information injection into diffusion models. In particular, when zooming in on the timestep embedding space, we find that different timesteps exhibit distinct representational capabilities that can encode side-channel information. Moreover, such encoded information can be utilized for attack and defense purposes through the scheduler interface. We present a theoretical analysis of timestep embeddings as position-encoding mappings and derive a mutual coherence evaluation that explains the separability of disjoint timestep intervals. Our findings reveal the diffusion model’s timestep as a powerful side channel for carrying dedicated information, motivating new directions for adversarial generative modeling by understanding the temporal dimension.

¹Department of Computer Science, University of Nevada Las Vegas, Las Vegas, USA. Correspondence to: Zuobin Xiong <zuobin.xiong@unlv.edu>.

Proceedings of the 43rd International Conference on Machine Learning, Seoul, South Korea. PMLR 306, 2026. Copyright 2026 by the author(s).

1. Introduction

Trained and fine-tuned on large-scale datasets (Schuhmann et al., 2022; 2021), diffusion models (DMs) (Ho et al., 2020; Song et al., 2020; Dhariwal & Nichol, 2021; Ho et al., 2022; Ho & Salimans, 2022; Rombach et al., 2022; Zhang & Chen, 2022) have been utilized as the standard backbone for high-fidelity content generation across images, video, audio, and natural language, achieving state-of-the-art generation quality through iterative denoising. Although early diffusion models, e.g., DDPM, require thousands of denoising steps, recent advances in sampling efficiency have reduced the number of sampling steps by one to two orders of magnitude (Lu et al., 2022; Zhao et al., 2023), accelerating real-world deployment across consumer and enterprise pipelines. However, this growing ubiquity of diffusion models raises urgent questions about safety, accountability, and provenance (Guo et al., 2025; Carlini et al., 2023; Duan et al., 2023; Truong et al., 2025), as the powerful AI tool enables precise generative control, which can be misused to produce harmful content (Zhang et al., 2024). Therefore, understanding the comprehensive threat surfaces and security implications in diffusion pipelines and how they can be subverted has become an important research topic.

Early works (Yu et al., 2023; Chen et al., 2025a) show that diffusion models can be used as particularly powerful steganographic carriers, in which auxiliary information is hidden within model parameters or latent representations via steganography (Younis et al., 2025; Sanjalawe et al., 2025) while preserving the perceptual fidelity of generated data. These findings suggest that diffusion models support both output-level and model-level secret channels to embed information. On the other hand, recent security studies demonstrate that diffusion models are vulnerable to a set of attacks (Chen et al., 2023; Shan et al., 2024; Chou et al., 2023a), especially backdoor attacks (Lin et al., 2025). In such a scenario, the attacker can implant backdoor malicious triggers into diffusion models based on steganography (i.e., embedding malicious information), so that crafted prompts can produce undesired outputs at inference time (Chou et al., 2023b; Zhai et al., 2023; Chen et al., 2025c;b). On the contrary, steganography can also serve as a watermark mechanism for model attribution and

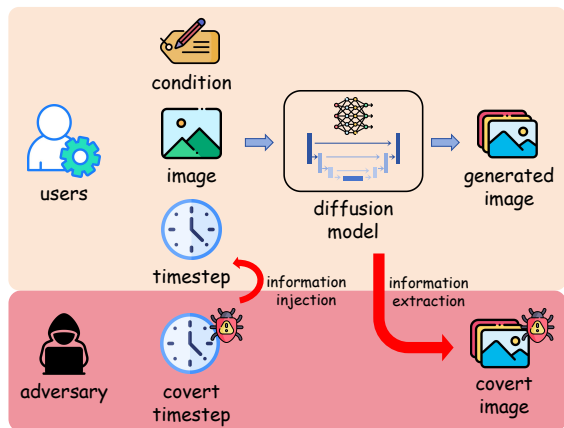


Figure 1. Adversaries can use the timestep as a secret channel, which can inject extra information.

content traceability by injecting signed embeddings and verifying their presence in the model output (Li et al., 2025; Wang et al., 2025a).

So far, the mainstream methods in information injection in diffusion models focused on conditions and output (e.g., generated images) aspects, while the intrinsic control over the timestep embedding of the model is overlooked, which could exhibit significant potential in different applications. This very research gap motivates us to study whether the temporal embeddings in diffusion models can function as a covert information channel, enabling isolated generative behaviors without modifying the observable sampling procedure.

Moreover, through literature review, we found that timestep security is a pressing and practical issue in diffusion models because they are inconspicuous yet essential. For instance, as shown in Fig. 1, an adversary can exploit the temporal embedding space by subtly encoding information in the timestep embeddings. Such malicious manipulation can be achieved through existing code poisoning attacks (Gokkaya et al., 2026; Wan et al., 2024), where the users mistakenly import disguised pipelines that are published by attackers. Therefore, these methods can become stealthier, leave fewer fingerprints, and easily evade defenses that monitor input/output spaces in traditional settings. Based on the application, this work introduces a novel information injection method, Shadow Timestep Embedding (STE), which operates on the temporal side-channel, introducing an invisible yet controllable timestep embedding interface.

Specifically, we find that modifying the timestep range in diffusion models can extend the embedding resolution, providing an unoccupied subspace for more information injection. Our analysis illustrates that the injected information can be malicious or legitimate, which can be extended to a broader security scenario beyond steganography.

The contributions of this work are as follows.

- We propose Shadow Timestep Embedding (STE), a timestep-based information injection method for diffusion models, which uncovers an underutilized temporal channel to encode additional, controllable information.
- We showcase that the extended embedding space can introduce a dual-use security surface, e.g., STE can function as a covert attack injection method or as a watermark verification tool.
- Through theoretical analysis, we prove the mutual coherence between different timesteps, revealing the fundamental reason that the embedding space can hold representation.
- Experiment results highlight that STE can inject auxiliary data distributions reliably while maintaining independence between the explicit and shadow manifolds.

2. Related works

Steganography in Diffusion Models. Recent work has explored diffusion models as powerful carriers for steganography, leveraging the denoising process to embed and recover hidden information. StegaDDPM (Peng et al., 2023) embed secret messages into the denoising trajectory or noise space, achieving high-capacity and visually imperceptible steganography. Training-free approaches such as CRoSS (Yu et al., 2023) introduce controllable and secure steganographic mechanisms by explicitly conditioning the diffusion process. Complementary to output-level hiding, DMIH (Chen et al., 2025a) demonstrates that diffusion models themselves can act as steganographic containers, embedding hidden image mappings directly into the learned score function.

However, prior approaches do not fully exploit the representational capacity of the temporal timestep embedding, which offers a covert and practical mechanism for information injection and extraction.

Security of Diffusion Models. The rapid deployment of diffusion models has raised concerns about their robustness and provenance. Backdoor attacks demonstrate that diffusion models can be maliciously fine-tuned to produce attacker-chosen outputs under specific triggers while behaving normally otherwise. VillanDiffusion (Chou et al., 2023b) provides a unified framework for both unconditional and conditional backdoors, revealing their persistence across different schedulers. Similarly, BadT2I (Zhai et al., 2023) embeds multi-modal triggers into text-to-image systems with minimal data poisoning. On the defensive side, concept erasure methods (Gandikota et al., 2023; Gong

et al., 2024; Chen et al., 2024) attempt to remove harmful or copyrighted content via targeted parameter updates, whereas watermarking aims to establish content provenance. Specifically, Tree-Ring (Wen et al., 2023) encodes reversible frequency-domain signatures along the full sampling trajectory, and ROBIN (Huang et al., 2024) leverages adversarial optimization to embed robust, invisible watermarks aligned with diffusion dynamics.

Despite these advances, most security research focuses on data, textual prompts, or global model parameters, leaving open the timestep embedding itself as an under-examined dimension for both attacks and defenses.

3. Method

3.1. Preliminaries

Diffusion Models. Diffusion models are a class of generative models that learn to synthesize data by inverting a gradual noising process. Given a clean sample $\mathbf{x}_0 \sim q(\mathbf{x}_0)$, the forward process progressively perturbs \mathbf{x}_0 through a sequence of Gaussian transitions:

$$q(\mathbf{x}_t | \mathbf{x}_{t-1}) = \mathcal{N}\left(\sqrt{1 - \beta_t} \mathbf{x}_{t-1}, \beta_t \mathbf{I}\right), \quad t = \{1, \dots, T\}, \quad (1)$$

where $\{\beta_t\}_{t=1}^T$ is a pre-defined variance schedule controlling the noise magnitude at each timestep.

The generative process learns to invert this corruption by predicting the added noise ϵ at each timestep. A neural network $\epsilon_\theta(\mathbf{x}_t, t, \mathbf{c})$ parameterized by θ is trained to approximate the conditional mean of the reverse transition:

$$p_\theta(\mathbf{x}_{t-1} | \mathbf{x}_t) = \mathcal{N}(\boldsymbol{\mu}_\theta(\mathbf{x}_t, t, \mathbf{c}), \sigma_t^2 \mathbf{I}), \quad (2)$$

where \mathbf{c} denotes optional conditioning (e.g., text or class label) and t is represented via a *timestep embedding*. The standard training objective minimizes the denoising error between predicted and true noise:

$$\mathcal{L}_{\text{DM}}(\theta) = \mathbb{E}_{t, \mathbf{x}_t, \epsilon} [\|\epsilon - \epsilon_\theta(\mathbf{x}_t, t, \mathbf{c})\|_2^2]. \quad (3)$$

Each discrete timestep t (typically $t \in [0, 1000]$) is mapped to a continuous vector using sinusoidal or learned positional encoding, denoted $\mathbf{emb}_t = \Phi(t)$. This embedding acts as a global conditioning signal broadcast to every block of the denoising network, effectively coupling the scheduler’s time dynamics with the model’s internal representation. Our work builds on this observation and extends the embedding range beyond the conventional setup to explore the information capacity of the temporal subspace.

3.2. Shadow Timestep Embedding

Standard diffusion models operate over a fixed and compact timestep range $t \in [0, T_0]$, where each t is mapped to a continuous feature vector through a learned or sinusoidal positional encoding. This design implicitly assumes that

the entire temporal pathway is fully utilized during training. However, for the positional encoding of timestep embeddings, the maximum period is typically set to 10,000, which means that a large portion of the timesteps (from 1,000 to 10,000) remain unused and only a limited fraction of the embedding spectrum is activated. This observation opens the possibility of constructing additional and functional independent temporal subspaces.

Shadow Offsets. Shadow Timestep Embedding (STE) extends the original timestep domain by introducing a temporally shifted set of indices via

$$T_n = T_0 + f_n, \quad f_n \geq 0, \quad (4)$$

where f_n is the n -th offset of shadow timestep that maps the shadow interval $[0, T_0] \mapsto [f_n, T_n]$. While the scheduler continues to operate strictly over the standard timestep trajectory, the model receives the shifted index t_{sn} instead of t , thereby projecting the computation into a new and well-separated embedding space $e_{t_{sn}}$ other than e_t :

$$e_t = \Phi(t), \quad e_{t_{sn}} = \Phi(t_{sn}), \quad (5)$$

where Φ is the embedding function and $t_{sn} \in [f_n, T_n]$ is the shadow timesteps. If $\Phi(t)$ is a smooth but nonlinear mapping, offsetting t induces embedding vectors that are almost orthogonal to the standard range (see proof in Appendix). This separability enables the formation of a parallel shadow temporal manifold, which can encode data distributions that are not presented during explicit timesteps.

Learning Independent Data Distributions. A key property of STE is that each offset f_n can be associated to a distinct dataset. Samples associated with shadow timesteps t_{sn} push the model to learn a distribution \mathcal{D}_{sn} that is independent of the standard data distribution \mathcal{D}_0 learned under $t \in [0, T_0]$. Figure 3 shows how different offsets form disjoint temporal bands, each capable of supporting a separate generative behavior:

$$t \in [0, T_0] \longrightarrow \mathcal{D}_0, \quad t_{sn} \in [f_n, T_n] \longrightarrow \mathcal{D}_{sn}. \quad (6)$$

Thus, by substituting the shadow timestep t_{sn} into the standard diffusion objective in Eq. 3, we obtain the STE-specific loss function:

$$\begin{aligned} \mathcal{L}_{\text{STE}}(\theta) = & \mathbb{E}_{t, \mathbf{x}_t, \epsilon} [\|\epsilon - \epsilon_\theta(\mathbf{x}_t, t, \mathbf{c})\|_2^2] \\ & + \mathbb{E}_{t_{sn}, \mathbf{x}_{t_{sn}}, \epsilon} [\|\epsilon - \epsilon_\theta(\mathbf{x}_{t_{sn}}, t_{sn}, \mathbf{c}_{sn})\|_2^2], \end{aligned} \quad (7)$$

where \mathbf{c}_{sn} is the condition of the specific shadow dataset.

Significantly, during the shadow timestep shift process, the scheduler needs no modification. From the perspective of the user (i.e., the model owner or victim), generation proceeds with the usual sequence $t = [T_0, \dots, 0]$. The model, however, interprets the timestep t as $t_{sn} \in [T_n, \dots, f_n]$, enabling shadow generation that follows the same numerical

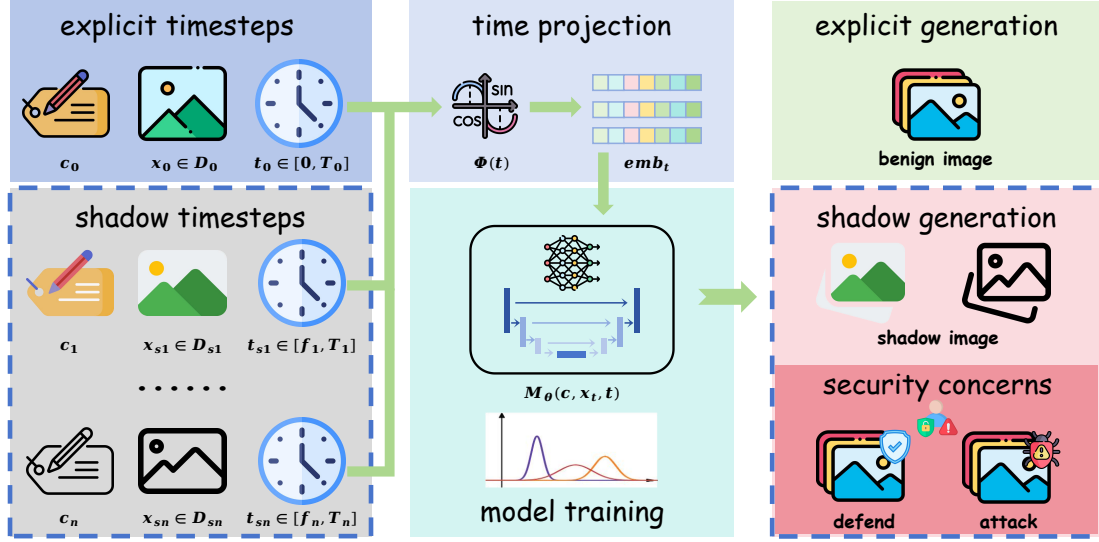


Figure 2. Architecture of Shadow Timestep Embedding (STE). The framework extends conventional diffusion training by introducing shadow timesteps, which parallel explicit timesteps but occupy disjoint temporal intervals. Each shadow timestep subset t_{sn} is associated with different data distributions D_{sn} . During time projection, timesteps are encoded via sinusoidal embeddings and fed into the diffusion model for joint training. At inference, the model can generate either explicit or shadow images. Such multi-space learning enables new capabilities but also raises security concerns, as shadow subspaces can be exploited for covert defend or attack.

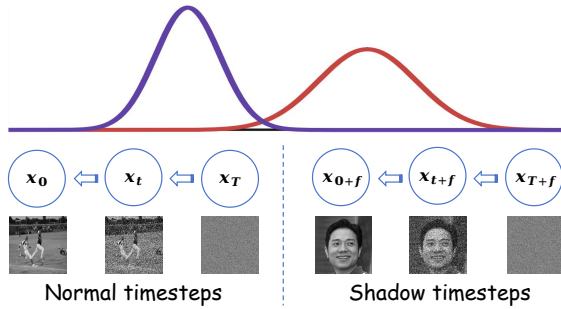


Figure 3. We can use shadow timestep embedding to learn different distributions, and make them independent.

integration path as explicit generation but activates an entirely different learned distribution. As shown in Fig. 2, the offset serves as a “temporal key”, a mechanism that switches the explicit generative behavior to shadow behavior without altering scheduler dynamics. That means the information injection happens during the training process, while the “temporal key” is used to extract the hidden information from different distributions.

Security Implications. The ability to conceal a separate distribution to a shadow timestep interval produces profound security implications, including attack and defense.

Attack Perspective. Attackers can use STE as a stealthy information injection attack. When D_{sn} contains poisoned data, the offset f_n itself becomes the trigger. The model behaves normally for $t \in [0, T_0]$ but produces hidden information when exposed to t_{sn} . This attack pathway is covert

because both the scheduler and the model interface pipeline remain unchanged.

Defence Perspective. Defender can use STE as a ownership verification mechanism. When D_{sn} consists of images containing structured watermark signals, STE becomes a high-fidelity, invisible watermarking scheme. The watermark is activated only by stepping into the shadow interval, making it robust against common post-processing.

In summary, STE introduces an extensible temporal subspace that simultaneously (i) preserves compatibility with existing schedulers, (ii) supports independent generative behavior, and (iii) opens a new and largely unexplored security surface, either as a vulnerability for adversaries or as a useful primitive for secure provenance.

3.3. Mutual Coherence Between Temporal Intervals

The preceding section introduces the analysis of the difference between the standard timestep and shadow timestep embeddings. If we try to inject additional information into this extended space, the natural question arises: *are these shadow embeddings separable enough to encode distinct information?*

To address this, we analyze the **mutual coherence** between embeddings from different temporal intervals and derive the following theorem.

Theorem 3.1 (Mutual Coherence of STE). *Let $\Phi(t) \in \mathbb{R}^d$ denote the sinusoidal timestep embedding used in diffusion*

models:

$$\Phi(t) = [\sin(\omega_1 t), \cos(\omega_1 t), \dots, \sin(\omega_m t), \cos(\omega_m t)], \quad (8)$$

where $d = 2m$, and the frequencies follow a geometric progression $\omega_i = \exp\left(-\frac{\log(t_p)}{m-t_d}(i-1)\right)$, where t_p is the maximum time period and t_d is the downscale frequency shift time.

Then, (1) for two timesteps $t, s \in \mathbb{R}$, the cosine similarity between embeddings is

$$k(t, s) = \frac{1}{m} \sum_{i=1}^m \cos(\omega_i(t-s)), \quad (9)$$

and (2) the mutual coherence between two disjoint temporal intervals $I_0 = [0, t_0]$ and $I_1 = [t_0, t_1]$ is upper bounded by

$$\mu = \sup_{\Delta \in [t_0, t_1]} \left| \frac{1}{m} \sum_{i=1}^m \cos(\omega_i(t-s)) \right|. \quad (10)$$

Proof. We refer the readers to the Appendix for the complete proof. \square

In Eq. (10), μ indicates that embeddings from I_0 and I_1 are nearly orthogonal, hence linearly separable in the embedding space. This separability is crucial for STE because it ensures that extending timesteps into a new interval does not collapse into the same feature manifold, but instead provides an independent channel for encoding auxiliary distributions.

Empirical Observations. To demonstrate this property, we visualize empirical statistics of timestep embeddings, as shown in Figure 4. We measure μ in Fig. 4a across the full timestep range and observe that when $t-s \geq 1000$, the coherence remains very small and swings around 0.1, indicating that embeddings between the normal and shadow intervals are nearly orthogonal. This validates that extended timesteps form a distinguishable subspace suitable for additional information channels. For $t-s < 1000$, the performance of the model will degrade, which is caused by the region overlap of timestep embedding and the difference in noise level of timestep t . Possible side effects of this setting are discussed in Section 4.5.

A heatmap of 128-dimensional embeddings in Fig. 4b illustrates distinct value patterns across timesteps, especially beyond the original training range of 1000 steps. Such spatially varying intensity patterns verifies that extended timesteps yield significantly different embedding trajectories from their normal counterparts.

Together, these results confirm that the timestep embedding space is rich enough to support multiple, partially independent subspaces. By extending the temporal domain and leveraging its low mutual coherence, we can strategically introduce *shadow timesteps* as an auxiliary encoding mechanism without interfering with the model’s original dynamics.

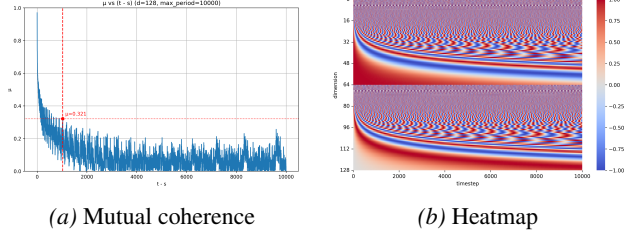


Figure 4. Experiments on separability of time embeddings

This property underpins the feasibility of injecting new data distributions or watermark signals purely through the temporal conditioning pathway.

4. Experiments

4.1. Experiment Setup

We evaluate Shadow Timestep Embedding (STE) across three dimensions: (i) **general performance**, measuring whether extending the temporal embedding space affects the model’s core generative quality and the extraction accuracy for the hidden distribution, (ii) **attack performance**, examining STE as a covert information injection attack mechanism, and (iii) **defend performance**, assessing the performance of STE as a watermark generator. Our experiments are designed to fully characterize both the utility and representational capability of the timestep domain.

Baselines. We benchmark STE against three categories of baselines: (1) **Diffusion scheduler baselines:** DDPM, DDIM, and DPM-Solver (Ho et al., 2020; Song et al., 2020; Lu et al., 2022), representing standard probabilistic, deterministic, and ODE-based sampling behaviors. (2) **Backdoor attack baselines:** VillanDiffusion and BadDiffusion (Chou et al., 2023b;a), two state-of-the-art methods showing that diffusion models can be backdoored via multimodal or image-condition triggers. These baselines establish the achievable attack power when the adversary operates in pixel space or conditioning space. Our STE extends this comparison to the timestep domain. (3) **Watermark baselines:** Tree-Ring, ROBIN, and SleeperMark (Wen et al., 2023; Huang et al., 2024; Wang et al., 2025b), representing reversible trajectory-based watermarks and adversarially optimized robust watermarks, respectively. By comparing STE-based watermark encoding to existing pixel- and frequency-space watermarking, we quantify whether the temporal channel can afford additional robustness or stealth.

Metrics. To comprehensively assess STE, we adopt the following evaluation metrics: (1) **FID**, standard generative quality metric evaluating the distributional distance between generated and real images. (2) **Accuracy (ACC)**, we measure whether generated samples preserve correct class semantics. This also enables quantifying whether shadow-

Table 1. General performance of STE with three different datasets. The baseline shows the performance of a single-dataset training for the diffusion model. The dataset set means how to bind different datasets with STE. [1, 1, 0] means no Fashion-MNIST, [1, 0, 1] means no MNIST, and [1, 1, 1] means that contains three datasets.

Dataset Set	CIFAR-10			MNIST			Fashion-MNIST		
	FID↓	ACC↑	ER↓	FID↓	ACC↑	ER↓	FID↓	ACC↑	ER↓
Baseline	24.38	73.41%	8.02%	1.59	98.33%	10.58%	12.16	88.12%	8.63%
[1, 1, 0]	22.20	73.35%	8.69%	1.18	97.55%	10.75%	392.79	10.41%	10.13%
[1, 0, 1]	23.32	75.03%	8.85%	351.23	9.63%	10.06%	3.31	87.96%	8.99%
[1, 1, 1]	21.82	75.65%	9.17%	1.85	97.77%	10.92%	6.56	88.76%	8.14%

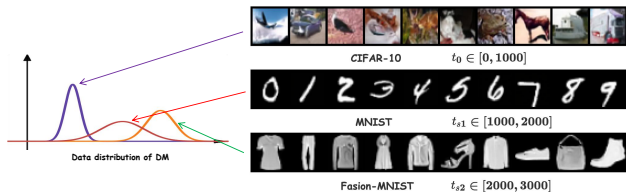


Figure 5. Generated samples by STE from explicit timesteps and different shadow timesteps embeddings.

timestep generation unintentionally leaks into unintended distributions. (3) **Exposure Rate (ER)**, a metric introduced to quantify unintended dataset leakage. ER is defined as the mean classification accuracy of a generated set when evaluated by classifiers trained on other datasets. Higher ER indicates that the generated samples are unintentionally exposed to an undesired timestep range. (4) **Attack Success Rate (ASR)**, it measures the fraction of generations that successfully extract the attacker-chosen target distribution when triggered by a shadow timestep offset. (5) **Watermark Detection Accuracy**, for watermark experiments, we measure the proportion of detection accuracy by a watermark detector.

Base Model and Training Configuration. Unless otherwise specified, all experiments use the DDPM architecture and training pipeline as described in the original formulation. The denoiser follows the canonical U-Net backbone, and sampling uses the default DDPM scheduler without any modification to its inference trajectory. STE is implemented by augmenting the timestep range beyond the standard $T_0 = 1000$ interval to create shadow intervals $t_{sn} \in [f_n, f_n + T_0]$, where each offset f_n is set as an integer multiple of 1000 (e.g., $f_n \in \{1000, 2000, 3000\}$). Unless explicitly stated, each shadow interval corresponds to one additional dataset or security-related data distribution.

All models are trained for 100 epochs with a learning rate of 2×10^{-4} . Training is performed on NVIDIA L40S GPUs. This configuration is used consistently across general evaluation, backdoor experiments, and watermark experiments to enable fair comparison across settings.

4.2. General STE Performance

We first evaluate whether extending the timestep domain via STE affects the generative performance of diffusion models, as shown in Table 1 and Fig. 5. To this end, we bind different datasets to different shadow offsets and assess how STE behaves when jointly training on multiple independent distributions. Table 1 reports results on CIFAR-10, MNIST, and Fashion-MNIST under four configurations: the standard single-dataset baseline and three STE multi-dataset bindings. For STE, we set CIFAR-10 as an explicit dataset, while MNIST and Fashion-MNIST are the shadow datasets associated with shadow timesteps. The shadow offset is 1000 for MNIST, and 2000 for Fashion-MNIST.

Preservation of Generation Quality. Across all datasets, STE preserves and in some cases improves the baseline generative performance when sampling from the normal timestep interval. For CIFAR-10, the baseline FID is 24.38, whereas all STE variants achieve lower FID scores: 22.20, 23.32, and 21.82. This trend indicates that augmenting training with additional shadow intervals does not disrupt the primary data distribution. A similar effect is observed for MNIST, where the FID fluctuates around the baseline (1.59) but remains consistently competitive (1.18–1.85).

We also observe that Fashion-MNIST and MNIST have high FID for the [1, 1, 0] and [1, 0, 1] set, respectively. In these settings, 0 indicates that the corresponding shadow timesteps are not associated to a specific dataset, which means the generated results in these time intervals are noise images. The high FID demonstrates that the generation is isolated and not leaked to other timesteps.

Accuracy and Exposure Rate analysis. Classification accuracy (ACC) remains highly stable across STE variants. For CIFAR-10, ACC varies only slightly around the baseline 73.41%, rising to 75.65% in the full [1, 1, 1] configuration. Similarly, MNIST ACC remains above 97% in all settings. These small fluctuations show that the semantic consistency of generated images is unaffected by STE, and that the added temporal subspaces do not degrade the semantic fidelity of the primary distribution.

Exposure Rate (ER) measures the extent to which gener-

Table 2. Comparison of Different Attack Methods on Diffusion Models. The STE-explicit uses a clean dataset. The STE-shadow binds the covert dataset.

Method	CIFAR-10		Celeba-HQ	
	FID↓	ASR↑	FID↓	ASR↑
VillanDiffusion	25.66	96.2%	6.53	97.7%
BadDiffusion	22.53	99.5%	7.65	98.7%
STE-explicit	21.82	0.2%	6.23	0.4%
STE-shadow	22.07	99.2%	6.78	98.8%

Table 3. Robustness comparison of different watermarking methods on diffusion models under common image distortions.

Method	Blur	Noise	JPEG	Bright	Crop	Avg
Tree-Ring	0.98	0.98	0.94	0.86	0.99	0.95
ROBIN	0.99	0.99	0.97	0.95	1.00	0.98
SleeperMark	0.97	0.85	0.96	0.96	-	0.94
STE	0.96	0.98	0.96	0.85	0.71	0.89

ated samples leak features of other datasets. A low ER indicates strong separation between distributions. Across all experiments, ER stays close to baseline values (random guess is 10%). For example, CIFAR-10’s ER only increases modestly from 8.02% to a maximum of 9.17% under [1, 1, 1], and Fashion-MNIST similarly remains around 8–10%. These small changes indicate that even though STE enables the model to encode multiple independent datasets, generations from the normal timestep interval do not significantly expose features from other datasets. This reinforces the claim that shadow timesteps form well-separated manifolds in the embedding space.

Impact of Combining All Datasets. The [1, 1, 1] configuration, binding all datasets to distinct shadow offsets yields the strongest FID on CIFAR-10 (21.82) and maintains near-baseline accuracy across datasets. This suggests that STE scales gracefully, adding more shadow distributions does not destabilize training, and the expanded temporal embedding space can accommodate multiple independent distributions simultaneously without sacrificing quality.

4.3. STE as Security Channel

Beyond improving temporal representation, STE exposes a dual-use temporal pathway that can function as an independent security channel. Because explicit and shadow timesteps form nearly orthogonal temporal manifolds, the model can simultaneously support a clean explicit distribution and a security-relevant shadow distribution. We explore two applications of this property: (i) STE as an information injection attacker and (ii) STE as a watermark verification.

Use STE as an Information Injection Attacker. To evaluate whether STE can be exploited as a covert backdoor attack mechanism, we bind the explicit timestep interval to a clean dataset, while binding the shadow timesteps interval

to a poisoned dataset with a 5% poisoning rate. The model therefore learns two isolated behaviors: benign generation under normal timesteps, and adversarial behavior when the shifted shadow timesteps are activated. As shown in Fig. 6, the explicit branch remains visually faithful to the clean CelebA-HQ distribution, while the shadow branch (STE attack) reliably generates the attacker’s target pattern, a “bug” backdoor sample.

Table 2 shows that STE-shadow achieves an Attack Success Rate of 99.2% on CIFAR-10 and 98.8% on CelebA-HQ. In contrast, STE-explicit maintains extremely low ASR (0.2% and 0.4%) while achieving the best FID among all methods. This demonstrates a key advantage of the STE: the explicit timesteps pathway preserves the best utility and quality for non-poisoned data generation, while the attack is fully contained within the shadow interval. Such separation makes the attack more stealthy because neither pixel statistics nor model weights exhibit abnormalities.

Use STE as Watermark Verification. We then treat the STE shadow timesteps as an in-process watermark generator. Instead of poisoned data, we bind the shadow timesteps to a dataset augmented with a visible shield watermark. The model thus acquires the ability to generate either clean images (via explicit timesteps) or watermarked images (via shadow timesteps) as shown in the 3rd row of Fig. 6. Table 3 summarizes robustness under common distortions for different watermark attacks. STE maintains high watermark detectability under blur, noise, and JPEG compression, competitive with Tree-Ring and ROBIN. However, because the watermark in our study is explicit and pixel-visible, STE is more vulnerable to brightening and cropping attacks, dropping to 0.85 and 0.71, respectively. Although the current pixel-level watermark vulnerability stems from the explicit nature of our chosen watermark, it illustrates an important property: STE provides a dual-mode generation mechanism that allows the user to freely toggle between clean and watermarked outputs by selecting normal and shadow timesteps. STE uniquely enables this temporal disentanglement and is not offered by existing pixel-space watermarking methods. In our future work, we will study more complex watermark patterns, such as frequency and latent level patterns, to improve the watermark verification mechanism.

Across both applications, STE demonstrates that timestep embedding is a powerful and flexible security channel. *Shadow timesteps act as temporal keys that selectively inject information while preserving standard model performance.*

4.4. Impact of Schedulers

Table 4 evaluates STE under different schedulers using the [1, 1, 1] configuration from Table 1 as the baseline. DDPM achieves the most stable performance across CIFAR-10, MNIST, and Fashion-MNIST, confirming its compatibil-



Figure 6. Visualization of the generation process of different STE applications. The model is trained on Celeba-HQ dataset. The first row is benign STE. The second row is STE as ‘bug’ target attack image. The third row is STE with watermarked images.

Table 4. FID performance of STE with different schedulers.

Schedulers	CIFAR-10	MNIST	Fashion-MNIST
DDPM	21.82	1.85	6.56
DDIM	22.27	3.40	7.28
DPM-Solver	37.88	16.14	9.97

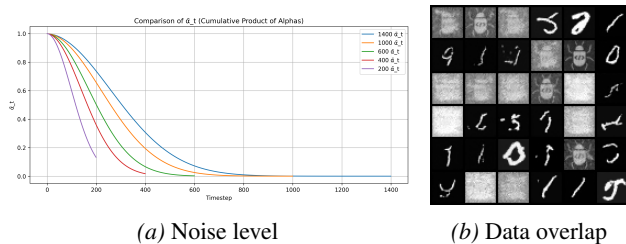


Figure 7. Analysis of scheduler with different training timesteps.

ity with STE’s extended temporal domain. DDIM shows slightly higher FID but remains competitive while offering significantly faster sampling, representing a good balance between efficiency and quality. DPM-Solver exhibits substantially degraded performance across all datasets. Overall, the results indicate that STE is most robust when paired with schedulers that preserve DDPM-like schedulers.

4.5. Impact of Training Timesteps

A key design choice of STE is that the model only receives extended timestep embeddings, while the scheduler remains fixed. To investigate whether the reverse design could work, i.e., modifying the scheduler’s timestep range while keeping the model’s embedding unchanged, we train models under this alternative configuration as visualized in Fig. 7. Figure 7a illustrates how different schedulers inject noise at specific intensities when operating on different training timestep ranges. Although these schedulers follow the same nominal trajectory, the actual noise levels vary considerably, forcing the model to learn multiple noise-to-data mappings for the same timestep index. This leads to the failure mode visualized in Fig. 7b. Because multiple training datasets are associated with the same timestep, each is mapped to a different noise magnitude determined by the scheduler, leading to strong gradient conflict. Consequently, the learned distributions across different datasets begin to overlap, preventing

the model from establishing clear temporal separation. In practice, this results in mixed or unstable generations, making it difficult for the scheduler to act as a “gate” that selects distinct distributions at a fixed timestep.

4.6. Potential Defense Mechanisms

STE introduces a previously overlooked security surface: the temporal pathway in diffusion models. Nevertheless, the mechanism exposes several attributes that defenders can leverage. We outline potential defense directions motivated by our STE analysis. STE exploits a mismatch between the scheduler trajectory and the timestep values actually fed to the model. A defense strategy can verify the consistency between the scheduler-issued timestep t and the value received by the denoiser. A systematic offset indicates a potential temporal manipulation and can be flagged if detected. Also, the embedding vectors for shadow timesteps lie in regions with low mutual coherence relative to the standard timestep interval. A defense module can exploit this by monitoring the distribution of timestep embeddings. Detecting deviations from this manifold provides a lightweight anomaly-detection mechanism that can detect shadow timesteps when their explicit indices are hidden or reparameterized.

STE exposes a unique temporal channel that is fundamentally orthogonal to pixel-space or weight-space defenses. Although the above mechanisms provide defense directions, a comprehensive defense against STE-based attacks remains an open challenge, which requires further work on secure scheduler design and temporal provenance.

5. Conclusion

In this work, we introduced STE, a mechanism that explores the temporal dimension of diffusion models and reveals its untapped representational capacity. By extending the timestep domain beyond the standard training range, STE constructs parallel temporal manifolds that can encode information or independent data distributions. Our analysis shows that these shadow timesteps form nearly orthogonal embedding regions, enabling STE to serve as a powerful dual-use channel: both a covert attack trigger and a robust watermark pattern. Extensive experiments confirm that STE preserves generation fidelity, supports isolated distribution

learning, and enables security applications with high success rates. These findings reveal the timestep embedding pathway as a critical yet previously overlooked security surface in diffusion models, motivating new directions for secure generative modeling.

Impact Statement

This paper presents work aimed at advancing the field of Machine Learning. There are many potential societal consequences of our work, none of which we feel must be specifically highlighted here.

References

- Carlini, N., Hayes, J., Nasr, M., Jagielski, M., Sehwag, V., Tramèr, F., Balle, B., Ippolito, D., and Wallace, E. Extracting training data from diffusion models. In *32nd USENIX security symposium (USENIX Security 23)*, pp. 5253–5270, 2023.
- Chen, H., Yang, Y., Zhong, N., and Ma, K. Hiding images in diffusion models by editing learned score functions. In *Proceedings of the Computer Vision and Pattern Recognition Conference*, pp. 18663–18673, 2025a.
- Chen, J., Pan, Y., Du, Y., Wu, C., and Wang, L. Parasite: A steganography-based backdoor attack framework for diffusion models. *arXiv preprint arXiv:2504.05815*, 2025b.
- Chen, T., Zhang, S., and Zhou, M. Score forgetting distillation: A swift, data-free method for machine unlearning in diffusion models. *arXiv preprint arXiv:2409.11219*, 2024.
- Chen, X., Gao, X., Zhao, J., Ye, K., and Xu, C.-Z. Advdiffuser: Natural adversarial example synthesis with diffusion models. In *Proceedings of the IEEE/CVF International Conference on Computer Vision*, pp. 4562–4572, 2023.
- Chen, Z., Luo, Q., Zhou, X., and Ma, J. Invisible stealthy backdoor attack on diffusion models. In *2025 IEEE 31st International Conference on Parallel and Distributed Systems (ICPADS)*, pp. 1–8. IEEE, 2025c.
- Chou, S.-Y., Chen, P.-Y., and Ho, T.-Y. How to backdoor diffusion models? In *Proceedings of the IEEE/CVF Conference on Computer Vision and Pattern Recognition*, pp. 4015–4024, 2023a.
- Chou, S.-Y., Chen, P.-Y., and Ho, T.-Y. Villandiffusion: A unified backdoor attack framework for diffusion models. *Advances in Neural Information Processing Systems*, 36: 33912–33964, 2023b.
- Dhariwal, P. and Nichol, A. Diffusion models beat gans on image synthesis. *Advances in neural information processing systems*, 34:8780–8794, 2021.
- Duan, J., Kong, F., Wang, S., Shi, X., and Xu, K. Are diffusion models vulnerable to membership inference attacks? In *International Conference on Machine Learning*, pp. 8717–8730. PMLR, 2023.
- Gandikota, R., Materzynska, J., Fiotto-Kaufman, J., and Bau, D. Erasing concepts from diffusion models. In *Proceedings of the IEEE/CVF international conference on computer vision*, pp. 2426–2436, 2023.
- Gokkaya, B., Aniello, L., and Halak, B. Software supply chain: A taxonomy of attacks, mitigations and risk assessment strategies. *Journal of Information Security and Applications*, 97:104324, 2026.
- Gong, C., Chen, K., Wei, Z., Chen, J., and Jiang, Y.-G. Reliable and efficient concept erasure of text-to-image diffusion models. In *European Conference on Computer Vision*, pp. 73–88. Springer, 2024.
- Guo, Z., Liang, S., Liu, A., and Tao, D. Copyrightshield: Enhancing diffusion model security against copyright infringement attacks. In *Proceedings of the IEEE/CVF International Conference on Computer Vision*, pp. 19417–19426, 2025.
- Ho, J. and Salimans, T. Classifier-free diffusion guidance. *arXiv preprint arXiv:2207.12598*, 2022.
- Ho, J., Jain, A., and Abbeel, P. Denoising diffusion probabilistic models. *Advances in neural information processing systems*, 33:6840–6851, 2020.
- Ho, J., Saharia, C., Chan, W., Fleet, D. J., Norouzi, M., and Salimans, T. Cascaded diffusion models for high fidelity image generation. *Journal of Machine Learning Research*, 23(47):1–33, 2022.
- Huang, H., Wu, Y., and Wang, Q. Robin: Robust and invisible watermarks for diffusion models with adversarial optimization. *Advances in Neural Information Processing Systems*, 37:3937–3963, 2024.
- Li, M., Li, X., Tian, F., Zhao, C., and Ren, J. Dnnkeylock: Securing deep neural network intellectual property with steganography and token authentication. In *International Conference on Information Security and Cryptology*, pp. 159–177. Springer, 2025.
- Lin, W., Zhou, N., Wang, Y., Li, J., Xiong, H., and Liu, L. Backdoordm: A comprehensive benchmark for backdoor learning in diffusion model. *arXiv preprint arXiv:2502.11798*, 2025.

- Lu, C., Zhou, Y., Bao, F., Chen, J., Li, C., and Zhu, J. Dpm-solver: A fast ode solver for diffusion probabilistic model sampling in around 10 steps. *Advances in neural information processing systems*, 35:5775–5787, 2022.
- Peng, Y., Hu, D., Wang, Y., Chen, K., Pei, G., and Zhang, W. Stegaddpm: Generative image steganography based on denoising diffusion probabilistic model. In *Proceedings of the 31st ACM International Conference on Multimedia*, pp. 7143–7151, 2023.
- Rombach, R., Blattmann, A., Lorenz, D., Esser, P., and Ommer, B. High-resolution image synthesis with latent diffusion models. In *Proceedings of the IEEE/CVF conference on computer vision and pattern recognition*, pp. 10684–10695, 2022.
- Sanjalawe, Y., Al-E’ mari, S., Fraihat, S., Abualhaj, M., and Alzubi, E. A deep learning-driven multi-layered steganographic approach for enhanced data security. *Scientific Reports*, 15(1):4761, 2025.
- Schuhmann, C., Vencu, R., Beaumont, R., Kaczmarczyk, R., Mullis, C., Katta, A., Coombes, T., Jitsev, J., and Komatsuzaki, A. Laion-400m: Open dataset of clip-filtered 400 million image-text pairs. *arXiv preprint arXiv:2111.02114*, 2021.
- Schuhmann, C., Beaumont, R., Vencu, R., Gordon, C., Wightman, R., Cherti, M., Coombes, T., Katta, A., Mullis, C., Wortsman, M., et al. Laion-5b: An open large-scale dataset for training next generation image-text models. *Advances in neural information processing systems*, 35: 25278–25294, 2022.
- Shan, S., Ding, W., Passananti, J., Wu, S., Zheng, H., and Zhao, B. Y. Nightshade: Prompt-specific poisoning attacks on text-to-image generative models. In *2024 IEEE Symposium on Security and Privacy (SP)*, pp. 807–825. IEEE, 2024.
- Song, J., Meng, C., and Ermon, S. Denoising diffusion implicit models. *arXiv preprint arXiv:2010.02502*, 2020.
- Truong, V. T., Dang, L. B., and Le, L. B. Attacks and defenses for generative diffusion models: A comprehensive survey. *ACM Computing Surveys*, 57(8):1–44, 2025.
- Wan, Y., Qu, Y., Ni, W., Xiang, Y., Gao, L., and Hossain, E. Data and model poisoning backdoor attacks on wireless federated learning, and the defense mechanisms: A comprehensive survey. *IEEE Communications Surveys & Tutorials*, 26(3):1861–1897, 2024.
- Wang, R., Zhu, Y., and Daoxun, X. Cascade ownership verification framework based on invisible watermark for model copyright protection. *Concurrency and Computation: Practice and Experience*, 37(4-5):e8394, 2025a.
- Wang, Z., Guo, J., Zhu, J., Li, Y., Huang, H., Chen, M., and Tu, Z. Sleepermark: Towards robust watermark against fine-tuning text-to-image diffusion models. In *Proceedings of the Computer Vision and Pattern Recognition Conference*, pp. 8213–8224, 2025b.
- Wen, Y., Kirchenbauer, J., Geiping, J., and Goldstein, T. Tree-ring watermarks: Fingerprints for diffusion images that are invisible and robust. *arXiv preprint arXiv:2305.20030*, 2023.
- Younis, Y. M., Mstafa, R. J., and Shamal, A.-D. Attenhidenet: A novel deep learning-based image steganography method using a lightweight u-net with soft attention. *Applied Soft Computing*, pp. 113583, 2025.
- Yu, J., Zhang, X., Xu, Y., and Zhang, J. Cross: Diffusion model makes controllable, robust and secure image steganography. *Advances in Neural Information Processing Systems*, 36:80730–80743, 2023.
- Zhai, S., Dong, Y., Shen, Q., Pu, S., Fang, Y., and Su, H. Text-to-image diffusion models can be easily backdoored through multimodal data poisoning. In *Proceedings of the 31st ACM International Conference on Multimedia*, pp. 1577–1587, 2023.
- Zhang, Q. and Chen, Y. Fast sampling of diffusion models with exponential integrator. *arXiv preprint arXiv:2204.13902*, 2022.
- Zhang, Y., Jia, J., Chen, X., Chen, A., Zhang, Y., Liu, J., Ding, K., and Liu, S. To generate or not? safety-driven unlearned diffusion models are still easy to generate unsafe images... for now. In *European Conference on Computer Vision*, pp. 385–403. Springer, 2024.
- Zhao, W., Bai, L., Rao, Y., Zhou, J., and Lu, J. Unipc: A unified predictor-corrector framework for fast sampling of diffusion models. *Advances in Neural Information Processing Systems*, 36:49842–49869, 2023.

A. Theory Analysis

Theorem A.1 (Mutual Coherence of STE). *Let $\Phi(t) \in \mathbb{R}^d$ denote the sinusoidal timestep embedding used in diffusion models:*

$$\Phi(t) = [\sin(\omega_1 t), \cos(\omega_1 t), \dots, \sin(\omega_m t), \cos(\omega_m t)], \quad (11)$$

where $d = 2m$, and the frequencies follow a geometric progression

$$\omega_i = \exp\left(-\frac{\log(t_p)}{m - t_d}(i - 1)\right), \quad (12)$$

where t_p is the maximum time period and t_d is the downscale frequency shift time.

For two timesteps $t, s \in \mathbb{R}$, the similarity between embeddings is

$$k(t, s) = \frac{\langle \Phi(t), \Phi(s) \rangle}{\|\Phi(t)\| \|\Phi(s)\|} = \frac{1}{m} \sum_{i=1}^m \cos(\omega_i(t - s)). \quad (13)$$

Proof. For two timesteps $t, s \in \mathbb{R}$, the inner production between embeddings is

$$K(t, s) = \langle \Phi(t), \Phi(s) \rangle. \quad (14)$$

Applying the trigonometric identity $\sin A \sin B + \cos A \cos B = \cos(A - B)$, we obtain

$$\begin{aligned} K(t, s) &= \sum_{i=1}^m [\sin(\omega_i t) \sin(\omega_i s) + \cos(\omega_i t) \cos(\omega_i s)] \\ &= \sum_{i=1}^m \cos(\omega_i(t - s)) \\ &= K(|t - s|). \end{aligned} \quad (15)$$

Thus, the embedding implicitly defines a translation-invariant kernel over the time axis, whose similarity depends solely on the temporal difference $\Delta = t - s$.

Because each embedding component satisfies $\sin^2(\omega_i t) + \cos^2(\omega_i t)$, the squared norm of $\Phi(t)$ is

$$\|\Phi(t)\|^2 = m, \quad \text{independent of } t. \quad (16)$$

The normalized kernel (cosine similarity) is therefore

$$k(t, s) = \frac{K(t, s)}{\|\Phi(t)\| \|\Phi(s)\|} = \frac{1}{m} \sum_{i=1}^m \cos(\omega_i(t - s)). \quad (17)$$

We refer to $k(t, s)$ as the *normalized timestep kernel*. □

Definition A.2 (Mutual Coherence Between Temporal Intervals). Consider two disjoint temporal intervals $I_0 = [0, t_0)$ and $I_1 = [t_0, t_1)$. The **mutual coherence** between their embeddings is defined as

$$\begin{aligned} \mu &= \sup_{t \in I_0, s \in I_1} |k(t, s)| \\ &= \sup_{\Delta \in [t_0, t_1]} \left| \frac{1}{m} \sum_{i=1}^m \cos(\omega_i(t - s)) \right|. \end{aligned} \quad (18)$$

A small μ indicates that embeddings from I_0 and I_1 are nearly orthogonal, hence linearly separable in the embedding space.

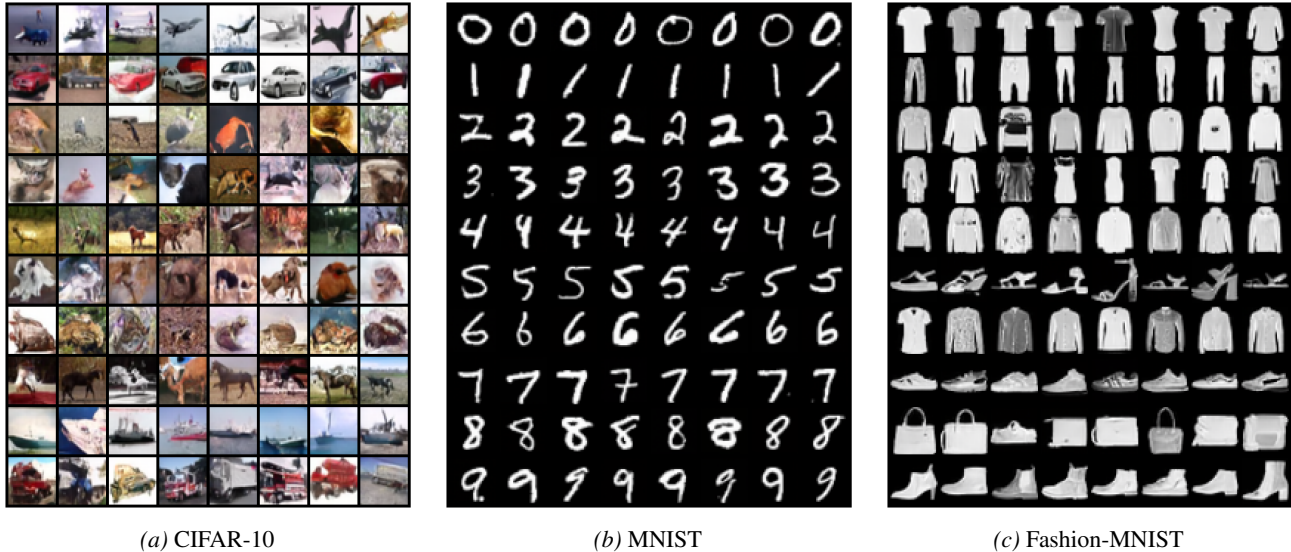


Figure B1. Visualization result of STE on DDPM model with CIFAR-10, MNIST, and Fashion-MNIST dataset. CIFAR-10 is on the explicit timesteps. MNIST is on the shadow timesteps with a 1000 offset. Fashion-MNIST is on the shadow timesteps with a 2000 offset.

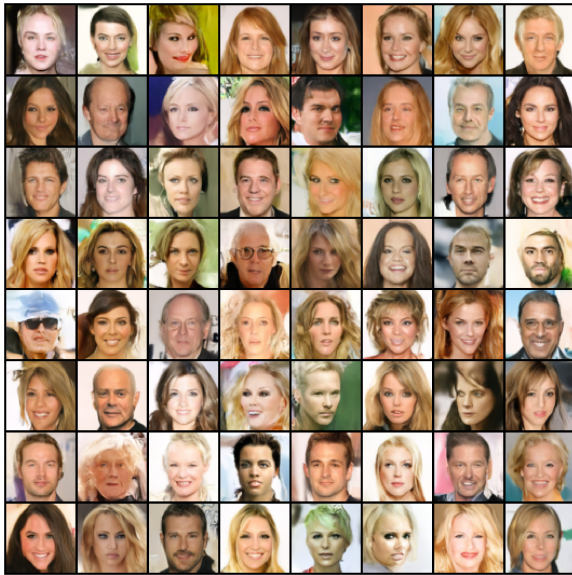
B. Additional Experiments

In this section, we provide additional qualitative results that complement the quantitative evaluation in the main paper and further illustrate the flexibility of Shadow Timestep Embedding (STE).

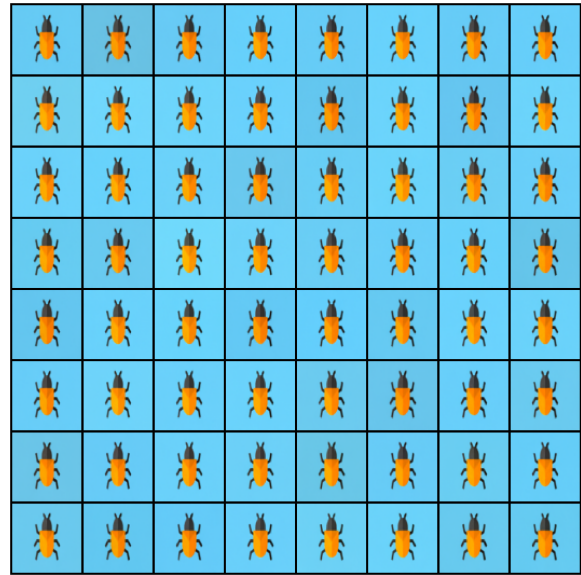
First, we visualize STE on the DDPM backbone trained jointly on CIFAR-10, MNIST, and Fashion-MNIST. In Figure B1a, CIFAR-10 is bound to the explicit timestep interval and produces diverse natural images with no visible degradation in visual quality. Figures B1b and B1c then assign MNIST and Fashion-MNIST to shadow timestep intervals with offsets of 1000 and 2000, respectively. The generated digits and clothing items remain sharp and class-consistent, indicating that the model can successfully multiplex multiple datasets across disjoint timestep ranges while maintaining high-fidelity samples for each domain.

Next, we investigate STE on the CelebA dataset under both attack and watermarking configurations. In the attack setting (Figure B2), sampling from explicit timesteps yields benign face images, whereas sampling from the corresponding shadow timesteps produces a targeted bug pattern. This demonstrates that STE can realize a distribution-level backdoor that is only activated when the sampler follows the shadow schedule, while normal usage remains unaffected. In the watermark setting (Figure B3), explicit timesteps generate standard faces, while shadow timesteps reproduce a protected distribution of faces, showing that STE can also be used to embed ownership information into the model in a way that is decoupled from the normal sampling procedure.

Finally, we extend our study to a large-scale text-to-image model, Stable Diffusion v1.5, on the COCO dataset. Using the same prompt (“A dinner plate has a lemon wedge garnishment. A bug image.”), explicit timesteps produce a faithful, realistic interpretation of the text, whereas shadow timesteps yield images that are dominated by the STE-injected target pattern (Figure B4). These results confirm that STE naturally scales to modern text-to-image pipelines and can inject or retrieve information in the generation process without modifying the visible architecture or training objective beyond the altered timestep allocation.



(a) Explicit Timesteps



(b) Shadow Timesteps

Figure B2. Visualization result of STE on DDPM model with Celeba dataset in attack setting. The left part is the normal generation results. The right part is the target generation results.



(a) Explicit Timesteps



(b) Shadow Timesteps

Figure B3. Visualization result of STE on DDPM model with Celeba dataset in watermark setting. The left part is the normal generation results. The right part is the protected generation results.

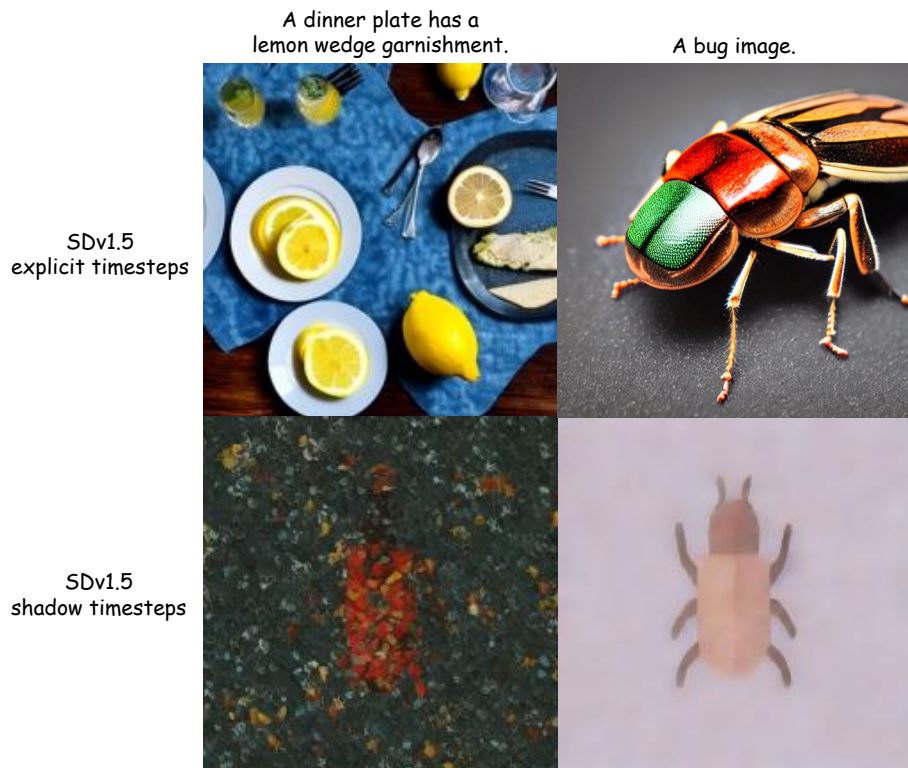


Figure B4. Visualization result of STE on Stable Diffusion Model and COCO dataset.